Химия растительного сырья. 2024. №2. С. 109–117.
Khimiya rastitel'nogo syr'ya, 2024, no. 2, pp. 109–117.
DOI: 10.14258/jcprm.20240213008

UDC 547.458.8:581.135.55

DISTINCTIVE FEATURES OF CELLULOSE NANOCRYSTALLITES

© ***M.Ya. Ioelovich***

Designer Energy Ltd, Bergman st., 2, Rehovot, 76100, Israel, ioelovichm@gmail.com

In this paper, a set of methods was used to study the structural characteristics and properties of cellulose nanocrystallites and free cellulose nanocrystalline particles (CNCs). It was shown that cellulose nanocrystallites have three main distinctive features. The first distinctive feature of cellulose nanocrystallites is their rod-like shape with a quite high aspect ratio and a low percolation threshold. The second distinctive feature of nanocrystallites is their highly developed specific surface area that leads to the spontaneous crystallization and aggregation of rod-like crystallites by their lateral planes. This aggregation process is thermodynamically favorable because it leads to a decrease in the specific surface area of nanocrystallites and a reduction of the thermodynamic potential. The third distinctive feature of cellulose nanocrystallites is the paracrystalline structure of their surface layers, which significantly affects structural characteristics such as lattice distortion, interplanar spacings, parameters, and volume of the crystalline unit cell, etc. Along with structure, the paracrystalline fraction affects also important physical and physical-chemical properties of cellulose, such as accessibility to deuteration, the content of CII-allomorph after cellulose alkalization, melting point of nanocrystallites, etc. Correlation equations were derived that provide to predict the structural characteristics and properties of nanocrystallites using the content of the paracrystalline fraction.

Keywords: cellulose, nanocrystallites, CNCs, distinctive features, structural characteristics, properties, correlations.

For citing: Ioelovich M.Ya. *Khimiya Rastitel'nogo Syr'ya*, 2024, no. 2, pp. 109–117. (in Russ.). DOI: 10.14258/jcprm.20240213008.

Introduction

As is known, cellulose is a semicrystalline natural polysaccharide that possesses a unique hierarchical architecture consisting of nano-scale fibrils built from nanocrystallites and noncrystalline nano-sized domains statistically alternated along the fibril [1, 2]. The three-dimensional well-ordered crystallites are strong and inaccessible constituents. However, the poorly ordered non-crystalline domains are weak and accessible places of the fibrils.

X-ray studies have shown that nanocrystallites of cellulose in plants have lateral sizes from 3–4 nm for the cellulose of herbaceous plants and woods to 5–6 nm for the cellulose of bast fibers (ramie, flax, etc.) and cotton [2, 3]. In the process of isolation from plant materials using various cooking methods, the lateral sizes of nanocrystallites increase due to the co-crystallization of neighboring crystallites by their lateral planes [3, 4]. As a result, the lateral sizes of crystallites of sulfite cellulose increase to 5–6 nm, and of Kraft cellulose to 6–7 nm. The largest lateral sizes, 15–20 nm, are observed for crystallites of cellulose isolated from tunicate and *Valonia* algae [5]. The length of nanocrystallites is in the range of 50 to 150 nm for nanocrystallites of plant celluloses [2]. However, the crystallites of tunicate and *Valonia* cellulose are much longer.

In addition to the X-ray method, the sizes of nanocrystallites can be studied by the methods of electron and atomic force microscopy. However, these microscopic methods require the preliminary isolation of nanocrystallites from cellulose using, e.g., acid hydrolysis. The cleavage of glycosidic bonds at the hydrolysis process occurs mainly in non-crystalline domains of cellulose nanofibrils that facilitate the obtaining of nanocrystalline particles called cellulose nanocrystals or cellulose nanocrystallites (CNCs) [6].

The mechanism of CNCs generation is unclear, and therefore it is a subject of discussion. This phenomenon is explained usually by selective acid hydrolysis of non-crystalline (amorphous) domains of cellulose nanofibrils, whereas the intact nano-crystallites can be isolated in the form of rod-like particles [7]. However, this mechanism does not explain, why the CNCs cannot be isolated in the case where the hydrolysis is performed by dilute acids (e.g., using 10–20 wt.% sulfuric acid or 8–10 wt.% hydrochloric acid) at boiling temperature despite achieving the LODP of cellulose [8]. As known, under these hydrolysis conditions, instead of CNCs, micro-scale cellulose parti-

cles of microcrystalline cellulose (MCC), are formed [9]. This is because cellulose nanocrystallites are joined together in lateral directions through strong crystalline contacts [10]. When the cellulose is hydrolyzed with the dilute acid, these contacts remain intact, and, instead of CNCs the MCC is obtained. To erode the strong inter-crystallite contacts, a sufficiently concentrated acid is required, e.g., 40–60 wt.% sulfuric acid (SA). For this purpose, the initial cellulose can be hydrolyzed with 60 wt.% SA at 45 °C or with 40 wt.% SA at 80 °C [11, 12]. To release CNCs the intensive mechanical or ultrasound disintegration of hydrolyzed cellulose in the aqueous medium is carried out. The formation of negatively charged sulfate groups on the CNCs surface after cellulose hydrolysis with concentrated sulfuric acid promotes electrostatic repulsion and leads to the phase stability of CNCs in aqueous dispersions.

Electron microscopic studies have shown that isolated CNCs are rod-shaped with a width of 5 to 50 nm and a length of 100 to 500 nm [2, 3, 7, 13, 14]. These CNCs have potential applications as thickeners, fillers, and reinforcements in papermaking, biodegradable materials, polymer composites, coatings, pharmaceutics, cosmetics, etc. [5, 11–14].

As is known, the characteristics of a certain type of macrocrystals, such as unit cell parameters, specific gravity, melting point, solubility, and others, are constant. However, as the size of crystals decreases down to the nano-scale, the laws of classical thermodynamics become inappropriate due to the significant contribution of the specific surface area to the thermodynamic functions [15]. This also applies to cellulose nanocrystallites. Therefore, the main purpose of this article was to show the distinctive features of cellulose crystallites and crystalline particles, CNCs, associated with their nano-sizes.

Experimental

Materials. Spruce wood sawdust (WS), Natural flax fibers (FF), Cotton linter (CL), Bleached sulfite pulp (BSP) of Weyerhaeuser, Bleached Kraft pulp (BKP) of Weyerhaeuser, Pure cotton cellulose (COC) of Hercules Inc., MCC Avicel PH-101 and lab microcrystalline celluloses, Tunicate Cellulose (TUC), and cellulose nano-crystallites (CNCs)

Wood cellulose was isolated from WS by the "soft" Kürschner-Hoffer (KH) delignification method [16], followed by bleaching with 1% $NaClO_2$ at pH=4, temperature 90 °C for 1 h, extraction with boiling 2% NaOH for 1 h, washing, and drying.

Kraft cooking of WS was carried out in a lab reactor at 170 °C, a liquor-to-WS ratio of 7 for 1, 2, and 3 h. The cooking liquor contained 8% NaOH and 2% Na_2S. After cooking, the isolated Kraft cellulose (KW) was washed, and dried.

To isolate cellulose from natural fibers, the samples of FF and CL were treated with 2% NaOH at 120 °C for 2 h, and then bleached, washed, and dried. TUC was isolated from *Halocynthia roretzi* by a two-stage cooking process using nitric acid and alkaline [17], followed by bleaching, washing, and drying.

Lab samples of microcrystalline cellulose (MCC) were obtained by hydrolysis of COC and BKP with boiling 2.5 N HCl for 60 min.

To prepare CNCs, the initial cotton cellulose (COC) was mixed with the needed amount of water in a lab flask, and then 80 wt.% SA was slowly added at cooling in an ice bath to obtain the final acid concentration of 40 wt.% and an acid-to-cellulose ratio of 10. The flask was placed into a water bath at temperature of 80 °C and treated while stirring for 60 min. After hydrolysis, the contents of the flask were poured out into a tenfold volume of cold water. The sediment of hydrolyzed cellulose was separated from the liquid phase by centrifugation at an acceleration of 5000 *g* for 10 min; washed with water, 1 wt.% sodium bicarbonate, and finally with distilled water to a pH of about 6, separating it from the water by centrifugation. To release CNCs, the washed sediment was diluted with distilled water to a concentration of 1 wt.% and disintegrated in an ultrasound disperser at 20 kHz and power of 400 W for 10 min at cooling in the ice bath. For X-ray studies, the CNCs dispersion was freeze-dried.

Methods

Content of alpha-cellulose. The content of alpha-cellulose in cellulose samples was analyzed according to the TAPPI T-203 standard method after treatment of the cellulose samples with 17.5% NaOH at 25 °C for 1h.

Wide-angle X-ray Scattering. X-ray measurements have been carried out on the "Rigaku Ultima Plus" diffractometer using CuKa radiation with a wavelength l =0.15418 nm in the 2Q-angle range from 5 to 80°. The collimation system consisted of vertical slits and Soller slits. A procedure of 0.02° step-by-step scanning was used

to determine the position of the peaks. The weak peaks were identified by a step-by-step scanning method with an accumulation of impulses at each step. The exact angular positions of the peaks were checked using a narrow line of NaF at 2Q of 38.83°. A few diffractograms of the same sample were recorded to obtain more reliable results. Then, X-ray patterns were improved using corrections on absorption, combined PL factor, and Rietveld refinement. Indexation of the reflections was made based of classical studies [18, 19]. Interplanar spacings of crystallites were calculated by the Bragg equation:

$$d = 0.5 \cdot l /(\sin Q), \quad (1)$$

Parameters of the crystalline unit cells (a, b, c) were calculated by standard equations comprising interplanar spacings (d_i) and Miller indices (h, k, l) of reflections [20]. For monoclinic unit cells of CI_β, these characteristics are related to each other by the following relation:

$$(1/d)^2 = (1/\sin\gamma)^2 [(h/a)^2 + (k/b)^2 + (l \sin\gamma/c)^2 - (2 hk \cos\gamma/ab)], \quad (2)$$

where γ is a monoclinic angle.

The actual size (D) of cellulose crystallites in a transverse direction perpendicular to [200]-planes was calculated by the equation [21]:

$$D = \lambda/[(\cos Q_{200})^2 (B_t^2 - b^2 - \Delta_t^2)]^{0.5}, \quad (3)$$

where B_t is the experimental integral broadening of the (200)-peak; b is the instrumental factor, $\Delta_t = 4\delta\, tgQ_{200}$ is the contribution of lattice distortions to the broadening of the (200)-peak, $\delta_t = \Delta d_t/d_{o,t}$ is the distortion parameter, $d_{o,t}$ = 0.384 nm is the undistorted spacing between [200]- planes.

The length (L) of crystallites perpendicular to [004]-planes was calculated from the equation [21]:

$$L = \lambda/[(\cos Q_{004})^2 (B_l^2 - b^2 - \Delta_l^2)]^{0.5}, \quad (4)$$

where B_l is the experimental integral broadening of the (004)-peak; b is the instrumental factor, $\Delta_l = 4\delta\, tgQ_{004}$ is the contribution of lattice distortions to the broadening of the (004)-peak, $\delta_l = \Delta d_l/d_{o,l}$ is the distortion parameter, $d_{o,l}$ = 0.260 nm is the undistorted spacing between [004]- planes.

The specific surface area (S) of rod-shaped nano-crystallites was calculated as follows:

$$S\ (m^2/g) = K/D, \quad (5)$$

where K=2470 is the dimension coefficient.

The percolation threshold of crystallites (Φ, vol. %) was found using the equation:

$$\Phi = c/AR, \quad (6)$$

where c=70 is the coefficient; AR=L/D is the aspect ratio [22].

The crystallinity (X) of cellulose samples was calculated from corrected X-ray patterns after removing the incoherent background and separating the crystalline scattering from the corrected X-ray pattern.

$$X = \int I_{cr}\, d2Q/\int I_o\, d2Q, \quad (7)$$

where I_{cr} is the intensity of the crystalline scattering and I_o is the total intensity of the corrected X-ray pattern.

Transmission electron microscopy (TEM). TEM of CNCs was carried out using a "Philips CM-200" electron microscope. The aqueous dispersion of CNCs after the homogenization step was diluted to 0.005% and treated with an ultrasound disintegrator. The diluted suspensions were dropped onto a carbon-coated grid and vacuum-dried. Then the sample was placed in the microscope, evacuated, and an electronic image was obtained.

Field emission scanning electron microscopy (FE-SEM). FE-SEM of dried CNCs was carried out using a “Hitachi S-4700” electron microscope. The diluted dispersion of dried CNCs (0.01%) was subjected to ultrasonic treatment for 5 min. A drop of the dispersion was applied onto a substrate and dried and the dry sample was coated

with a thin layer of gold. Then the sample was placed in the microscope, evacuated, and an electronic image was obtained.

Alkalization. The alkalization of cellulose samples was carried out with 12% sodium hydroxide at 25 °C, liquid-to-solid ratio 20 for 1h. The CII content was determined by the X-ray method of inner standard [17].

Deuteration of cellulose samples. Cellulose samples were treated with heavy water (D_2O) at 25 °C, D_2O-to-cellulose ratio of 10 for 24 h. After removing the excess heavy water, the treated samples were dried in a P_2O_5 – desiccator at 25 °C for 24 h and then in a drying chamber at 105 °C up to constant weight.

Pulse NMR. Dry cellulose samples were tested with a proton NMR apparatus operating at 42 MHz, with a 2.5 ms interval of the p/2 – pulse. The amplitudes of protons induction for the initial (I_o) and deuterated (I_d) cellulose samples were measured. The accessibility of cellulose samples upon deuteration was calculated by the equation [23]:

$$A = k\,[1-(I_d/I_o)], \tag{8}$$

where k=3.334 is the coefficient.

Results and discussion

The X-ray patterns of the natural cellulose were typical of a crystalline allomorph of CI_β with characteristic peaks at 2Θ angles of 14.5–15.0, 16.0–16.5, 22.4–22.8, and 34.5–34.7° due to X-ray diffraction from planes of the crystalline lattice with Miller indices of (1$\bar{1}$0), (110), (200), and (004), respectively [24] (Fig. 1).

As a result of X-ray studies, the various characteristics of the crystalline structure were calculated (Table 1).

From Table 1, it follows that the length of cellulose nanocrystallites is 10–30 times greater than their lateral size. Therefore, the first distinctive feature of cellulose nanocrystallites is that they are rod-shaped with an aspect ratio (AR) of 10 to 30, which gives a percolation threshold of 2 to 7%. Such a relatively small percolation threshold provides the formation of hydrogels and continuous networks in polymer nanocomposites at low content of cellulose nanocrystallites [25].

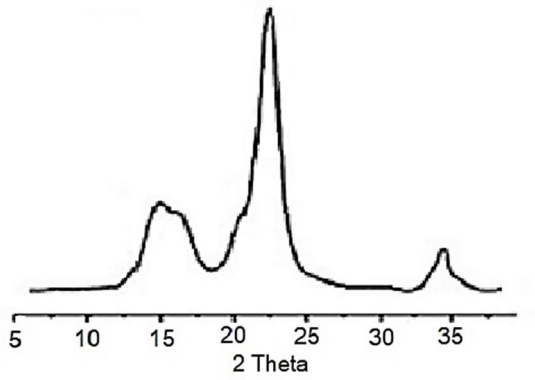

Fig. 1. X-ray pattern of COC sample

Table 1. Characteristics of the crystalline structure of studied samples

Samples	Abbr	X	L, nm	D, nm	d_t, nm	δ_t	α_p
Wood sawdust	WS	nd	80	3.8	0.395	0.033	0.38
Cellulose isolated from WS by KH method	KHWC	0.62	80	4.2	0.394	0.030	0.34
Cellulose isolated from WS by Kraft pulping	KWC	0.64	83	6.5	0.392	0.020	0.23
Natural Flax fibers	FF	0.66	90	5.1	0.393	0.025	0.29
Cellulose isolated from FF by natron pulping	FFC	0.69	92	6.0	0.392	0.021	0.25
Cotton linter	CL	0.68	98	5.7	0.392	0.023	0.26
Cellulose isolated from CL by natron pulping	CLC	0.70	100	6.5	0.391	0.020	0.23
Bleached sulfite pulp	BSP	0.63	86	6.3	0.392	0.021	0.24
Bleached Kraft pulp	BKP	0.65	88	7.0	0.391	0.018	0.21
Pure cotton cellulose	COC	0.71	110	7.6	0.390	0.017	0.20
MCC from BKP	BKM	0.73	94	7.8	0.390	0.016	0.19
MCC from COC	COM	0.74	112	9.0	0.389	0.014	0.16
MCC Avicel	AVM	0.75	116	9.4	0.389	0.013	0.15
Tunicate cellulose	TUC	0.80	400	13.0	0.388	0.010	0.12

Note: Abbr denotes an Abbreviation; nd denotes not determined

Nanocrystallites of cellulose in WS have a relatively small lateral size with D=3.8 nm. However, after cellulose isolation by various cooking methods, the lateral sizes of nano-crystallites increase, to a lesser extent in the case of the "soft" KH method, but to a larger extent in the case of natron and Kraft cooking.

This phenomenon can be clearly illustrated by the change in the X-ray pattern of cellulose after cooking plant material. Figure 2 shows that after the Kraft pulping of the WS sample, the (200)-peak of CI_β becomes more intensive and narrower, which indicates an increase in the lateral size of crystallites.

As is known [3], in various plants, cellulose nanocrystallites are surrounded by an amorphous lignin-hemicellulose matrix (LHM) preventing their direct contact. During the cooking of the raw material, this matrix is removed, which allows the crystallites of neighboring nanofibrils to contact each other with their lateral planes. When the necessary conditions are reached, the process of co-crystallization (twinning) of neighboring crystallites by their lateral planes occurs, which leads to an increase in the lateral size of crystallites. The degree of lateral crystallization (LCD, %) can be estimated by the equation:

$$LCD = 100\ [(D_c/D_p)-1], \tag{9}$$

where D_p and D_c are the actual lateral sizes of nanocrystallites in plant material and in isolated cellulose respectively.

The process of lateral crystallization can be implemented due to the second distinctive feature of cellulose nanocrystallites. This feature consists of a highly developed specific surface area (S) of rod-shaped nanocrystallites, which is especially large for crystallites with small lateral sizes, D (Fig. 3).

For this reason, nanocrystallites are thermodynamically unstable structures because their thermodynamic potential (G) is high. To order to transit to an equilibrium state, this potential must decrease by reducing the specific surface area, as follows:

$$\Delta G = \sigma\ \Delta S < 0, \tag{10}$$

where σ is the surface energy of crystallites.

In practice, this thermodynamic condition can be realized by lateral crystallization of rod-shaped nanocrystallites, leading to a decrease in their S-value. However, to implement this process, along with the thermodynamic condition, the kinetic condition must also be satisfied, namely, a sufficiently high temperature and a plasticizing medium are required to ensure increased segmental mobility of non-crystalline domains of cellulose nanofibrils and thereby facilitate contact between the surfaces of neighboring crystallites with each other. Therefore, the "hard" conditions of Kraft cooking, high temperature, and plasticizing alkaline medium, promote lateral crystallization of cellulose nanocrystallites, while under the "soft" conditions of the KH-method proceeding at a moderate temperature and poor plasticizing ethanol medium, the lateral crystallization is carried out to a small extent.

A detailed study of Kraft cooking of WS at 170 °C showed that at least three hours are required to remove the LHM and increase the degree of lateral crystallization (Table 2).

The industrial sample of bleached Kraft pulp is characterized by a higher value of LCD=87% than the laboratory sample LCD=71%. Since the process of lateral crystallization is facilitated by the high specific surface area of the crystallites, small nanocrystallites of wood cellulose more readily form twinned crystallites during cooking than larger nanocrystallites of flax or cotton. The process of lateral crystallization continues during the subsequent hydrolysis of isolated cellulose, which is carried out to obtain MCC and CNCs (Table 3).

TEM studies have shown that CNCs are rod-like (Fig. 4) with the most probable width (W) of 20 nm (Fig. 5).

Since the average width of the CNCs is almost twice the lateral size of nanocrystallites, these results indicate that the CNCs are nano-scale aggregates that are probably formed due to the adhesion of surface layers of several nanocrystallites. The spontaneous aggregation of free nanocrystallites is thermodynamically favorable because it leads to a decrease in the specific surface area and a reduction of the thermodynamic potential.

However, after conventional drying of aqueous dispersions of CNCs, intensive forced aggregation of nanoparticles occurs with the formation of micron-sized aggregates that remain even after ultrasonic treatment (Fig. 6).

The freeze-drying of CNCs dispersions also cannot prevent the formation of micro-scale aggregates [26]. This creates a problem when using dried CNCs as fillers in the production of composite materials.

The third distinctive feature of cellulose nanocrystallites is the paracrystalline structure of their surface layers, which significantly affects the structural characteristics of crystallites [23]. The content of the paracrystalline fraction in crystallites can be calculated, as follows:

$$\alpha_p = 4h\ (D\text{-}h)/D^2, \tag{11}$$

where h=0.4 nm is the thickness of the paracrystalline layer.

The content of such paracrystalline fraction in nanocrystallites can be quite significant and reach 40% for small crystallites with D of 3.5–3.6 nm. Since the paracrystalline fraction of a nano-crystallite has a highly distorted lattice, it was reasonable to establish its effect on the distortion degree of the crystalline lattice as a whole. It follows from Figure 7 that the parameter of crystalline lattice distortion (δ_t) is a linear function of the content of the paracrystalline fraction (α_p) in the crystallite:

$$\delta_t = \delta_p\ \alpha_p, \tag{12}$$

where δ_p is the distortion parameter of the paracrystalline lattice.

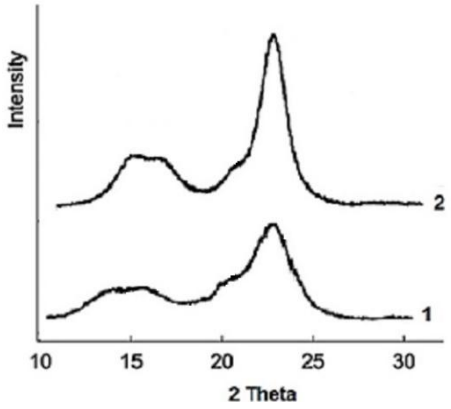

Fig. 2. X-ray patterns of wood sawdust (WS) (1) and Kraft cellulose isolated from WS (2)

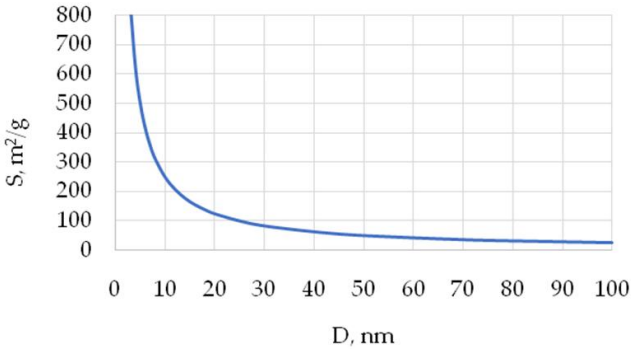

Fig. 3. Dependence of specific surface area of nanocrystallites on their lateral sizes calculated by eq. (5)

Table 2. Influence of Kraft cooking time of WS on the degree of lateral crystallization of nanocrystallites

Time, h	Alpha-cellulose, %	D, nm	LCD, %
0	nd	3.8	0
1	86	5.7	50
2	90	6.1	61
3	93	6.5	71
4	93	6.5	71

Table 3. The degree of additional lateral crystallization (LCD_a) during the production of MCC and CNCs

Sample	D, nm	LCD_a, %
BKM	7.8	11
COM	9.0	18
AVM	9.4	24
CNCs	10.1	33

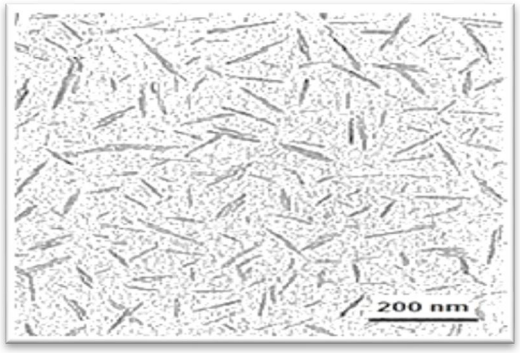

Fig. 4. TEM image of CNCs

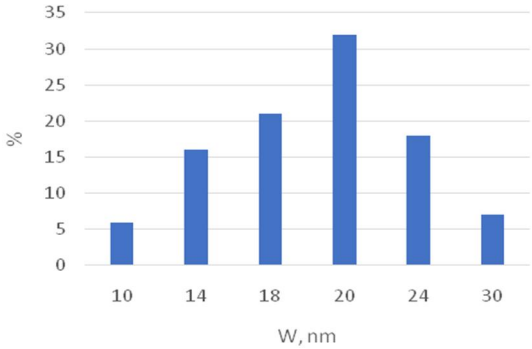

Fig. 5. Width distribution of CNCs

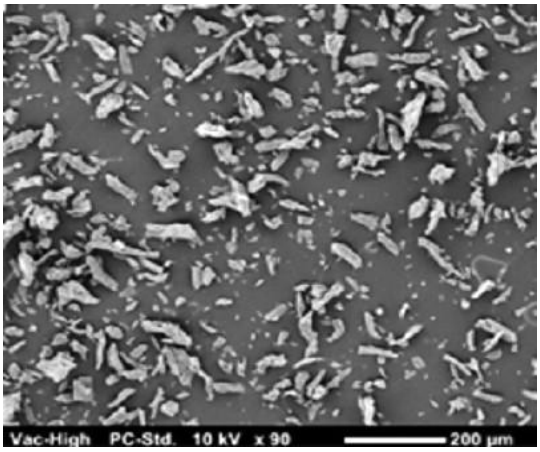

Fig. 6. SEM image of aggregates of dried CNCs

Thus, the distortion of the CI_β crystalline lattice was caused mainly by the contribution of the paracrystalline fraction. The content of the paracrystalline fraction decreases with an increase in the lateral size of crystallites, and therefore, the distortion of the crystallite lattice also decreases while the lateral size of the crystallites rises.

Since the content of the paracrystalline fraction determines the lattice distortion, this parameter also affects other structural characteristics of nanocrystallites, such as interplanar spacings (d_t), parameters (a, b), and volume (V_c) of the crystalline unit cell (Fig. 8–10).

The content of the paracrystalline fraction affects not only the structure but also important physical and physical-chemical properties of nanocrystallites, such as accessibility to deuteration (A), the content of CII-allomorph (CII) after alkalization of CIβ with 12% NaOH, melting point (Tm) of nanocrystallites, etc.

The studies have shown that the dependences of various structural characteristics and properties on the content of the paracrystalline fraction in the nanocrystallites can be described by the following correlation equations (Table 4).

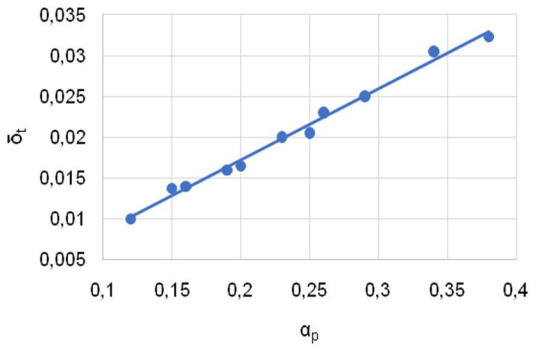

Fig. 7. Dependence of transverse distortion parameter on the content of paracrystalline fraction

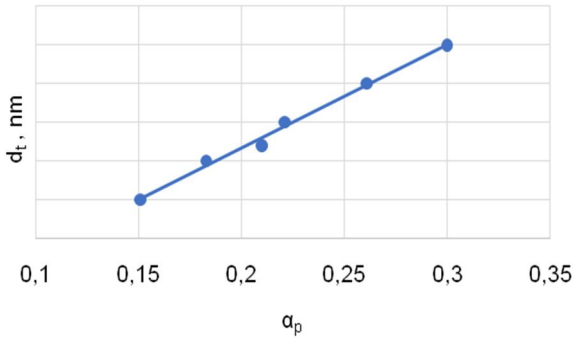

Fig. 8. Dependence of interplanar spacing on the content of paracrystalline fraction

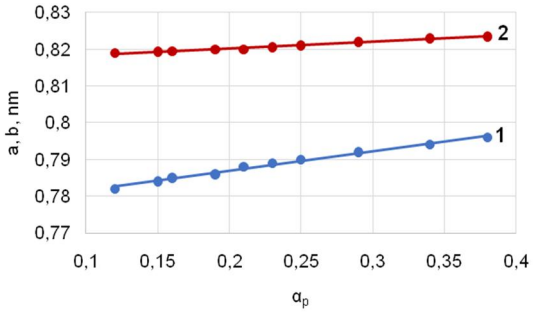

Fig. 9. Effect of paracrystalline fraction on parameters a (1) and b (2) of CI_β crystalline unit cell

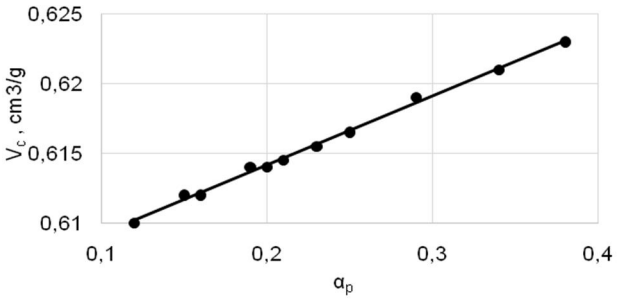

Fig. 10. Effect of paracrystalline fraction on the specific volume of cellulose crystallites

Table 4. Correlation equations

Function	Equation	R^2
$\delta_t = F(\alpha_p)$	$\delta_t = 0.087\ \alpha_p$	0.985
$d_t = F(\alpha_p)$	d_t (nm) = 0.384 + 0.032 α_p	0.987
$V_c = F(\alpha_p)$	V_c (cm^3/g) = 0.604 + 0.06 α_p	0.974
$A = F(\alpha_p)$	$A = 0.075 + 1.83\ \alpha_p$	0.982
$CII = F(\alpha_p)$	CII (%) = 500 α_p - 65	0.961
$T_m = F(\alpha_p)$	T_m (K) = 740 - 550 α_p	0.980

Conclusions

It was shown that cellulose nano-crystallites have three main distinctive features. The first distinctive feature of cellulose nanocrystallites is their rod-like shape with a quite high aspect ratio and a low percolation threshold ranging from 2 to 7%. Thus, the formation of hydrogels and continuous networks in polymer nanocomposites can be implemented using a relatively small addition of nanocrystallites.

The second distinctive feature of nano-crystallites is their highly developed specific surface area, which is especially large for crystallites with small lateral sizes. This feature facilitates the spontaneous crystallization and aggregation of rod-shaped crystallites by their lateral planes. The spontaneous aggregation of nanocrystallites is thermodynamically favorable because it leads to a decrease in the specific surface area and a reduction of the thermodynamic potential.

In various plants, cellulose nanocrystallites are surrounded by an amorphous lignin-hemicellulose matrix preventing their direct contact. During the cooking of the plant material, this matrix is removed, which allows the crystallites of neighboring nanofibrils to contact each other with their lateral planes. As a result, the process of lateral crystallization (twinning) of neighboring crystallites occurs, which leads to an increase in the lateral size of crystallites. The process of lateral crystallization continues during the subsequent hydrolysis of isolated cellulose to produce MCC and CNCs. The results also have shown that the CNCs are nano-scale aggregates that are probably formed due to the adhesion of surface layers of several nanocrystallites. However, after drying of aqueous dispersions of CNCs, the forced aggregation of nanoparticles occurs with the formation of aggregates of micron sizes. This creates a problem when using dried CNCs as fillers in the production of composite materials.

The third distinctive feature of cellulose nanocrystallites is the paracrystalline structure of their surface layers, which significantly affects structural characteristics such as lattice distortion, interplanar spacings, parameters, and volume of the crystalline unit cell, etc. Along with structure, the paracrystalline fraction affects also important physical and physical-chemical properties of cellulose, such as accessibility to deuteration, the content of CII-allomorph after cellulose alkalization, melting point of nanocrystallites, etc. Correlation equations were derived that provide to predict the structural characteristics and properties of nanocrystallites using the content of the paracrystalline fraction.

Funding
This work was supported funding Designer Energy Ltd. No additional grants to carry out or direct this particular research were obtained.

Conflict of Interest
The author of this work declares that he has no conflicts of interest.

References

1. Krässig H. *Cellulose: Structure, Accessibility and Reactivity*. Amsterdam: Gordon and Breach Publishers, 1996, 376 p.
2. Ioelovich M. *J. Polym. Sci. Ser. A*, 2016, vol. 58, pp. 925–943.
3. Ioelovich M. *Cellulose Nanostructured Natural Polymer*. Saarbrücken: Lambert Academic Publishing, 2014, 88 p.
4. Ioelovich M. *Wood Chem*., 1991, vol. 4, pp. 27–33.
5. Moon R., Martini A., Nairn J. et al. *Chem. Soc. Rev*., 2011, vol. 40, pp. 3941–3994.
6. Eichhorn S.J., Etale A., Wang J. et al. *J. Mater. Sci*., 2022, vol. 57, pp. 5697–5767.

7. Habibi Y., Lucia L.A., Rojas O.J. *Chem. Rev*., 2010, vol. 110, pp. 3479–3500.
8. Ioelovich M., Leykin A. *Cellul. Chem. Technol.*, 2006, vol. 40, pp. 313–317.
9. Yulina R., Gustiani S., Kasipah C., Sukardan M.D. *E3S Web of Conf*., 2020, vol. 148, pp. 1–6.
10. Ioelovich M. *SITA*, 2016, vol. 18, pp. 72–77.
11. Ioelovich M. *J. Chem. Educ. Res. Pract.*, 2017, vol. 1, pp. 1–6.
12. Ioelovich M. *Adv. Env. Waste Manag. Recycling*, 2020, vol. 3, pp. 128–132.
13. Kargarzadeh H., Ioelovich M., Ahmad I. et al. *Handbook of Nanocellulose and Cellulose Nanocomposites*. Singapore: Wiley, 2017, vol. 1-1, pp. 1–50.
14. Ioelovich M. *Handbook of Nanocellulose and Cellulose Nanocomposites*. Singapore: Wiley, 2017, vol. 1-2, pp. 51–100.
15. Ioelovich M. *Bioresources*, 2008, vol. 3, pp. 1403–1418.
16. Drożdżek M., Zawadzki J., Zielenkiewicz T., Kłosińska T. *Wood Res*., 2015, vol. 60, pp. 255–262.
17. Ioelovich M. *Chem. Res. J*., 2017, vol. 2, pp. 58–67.
18. Woodcock C., Sarko A. *Macromolecules*, 1980, vol. 13, pp. 1183–1187.
19. Sugiyama J., Vuong R., Chanzy H. *Macromolecules*, 1991, vol. 24, pp. 4168–4175.
20. Stout G.H., Jensen L.H. *X-ray Structure Determination: A Practical Guide*. New York: Wiley, 1989, 480 p.
21. Ioelovich M. *Progress in Characterization of Cellulose and Cellulose Esters*. Chisinau: Eliva Press, 2023, 80 p.
22. Dufresne A. *J. Nanosci. Nanotechnol*., 2006, vol. 6, pp. 322–330.
23. Ioelovich M., Leykin A., Figovsky O. *Bioresources*, 2010, vol. 5, pp. 1393–1407.
24. Simon M., Fulchiron R., Gouanvé F. *Polymers*, 2022, vol. 14, p. 2836.
25. Ioelovich M. *World J. Adv. Eng. Technol. Sci.*, 2022, vol. 5, pp. 1–15.
26. Han J., Zhou C., Wu Y. et al. *Biomacromolecules*, 2013, vol. 14, pp. 1529–1540.

Received May 30, 2023

Accepted January 12, 2024

Information about author

Ioelovich Michael Yacob – Professor, Chief Chemist, Head of Chemical Dep., ioelovichm@gmail.com